Radiation Physics and Chemistry 229 (2025) 112435

Contents lists available at ScienceDirect

Radiation Physics and Chemistry

journal homepage: www.elsevier.com/locate/radphyschem

Feasibility study of the use of a silicon photomultiplier coupled to a scintillator for kVp measurement based on spectrometry

Jonathan Rodrigues da Silva [a,*], Helio Massaharu Murata [a], Leonardo Camargo dos Santos [b], Juan Antonio Alcántara Núñez [b], Diego Vergaças de Souza Carvalho [b], Adelson Duarte dos Santos [b], Ubaldo Baños Rodríguez [b], Maria da Penha Albuquerque Potiens [b], Daniel Alexandre Baptista Bonifacio [b]

[a] Medical Physics Department, Radioprotection and Dosimetry Institute / Brazilian Nuclear Energy Commission (IRD/CNEN), Rio de Janeiro, Brazil
[b] Radiation Metrology Center, Nuclear and Energy Research Institute / Brazilian Nuclear Energy Commission (IPEN/CNEN), São Paulo, Brazil

ARTICLE INFO

Handling Editor: Dr. Chris Chantler

Keywords:
Silicon photomultiplier (SiPM)
GaGG scintillator crystal
Peak voltage (kVp)
Non-invasive measurement
Diagnostic radiology

ABSTRACT

This study proposes a spectroscopic and non-invasive approach to measure the kVp of an X-ray tube using a silicon photomultiplier (SiPM) coupled to a GaGG scintillator crystal. Several experimental setups were explored to assess the feasibility and performance in measuring the kVp based on international standards IEC 61267:2005 and IEC 61676:2002. The energy spectrum was obtained through pulse height analysis. System calibration was performed using radioactive sources emitting characteristic X-rays and gamma radiation. Determination of the maximum energy of the X-ray spectrum was based on a linear regression aiming for a goodness of the fit to reduce uncertainty in kVp. The approach was successfully evaluated for specific radiology beams, including mammography, with a maximum uncertainty of 6.5% in the kVp values for the tested beam qualities.

1. Introduction

One of the factors affecting the image quality in radiology is the mismatch between the voltage applied to the X-ray tube and the value set by the equipment (Fajrin et al., 2019). Measurement instruments are used to reduce possible deviations and to guarantee that the requirements of technical standards are respected, such as the accuracy and reproducibility of the measured voltage (AGENCY, 2023; BRASIL, 2022; IAEA, 2021).

The voltage applied to the X-ray tube can be directly quantified in an invasive manner using a meter integrated into the circuitry, enabling direct calibration and providing extremely reliable measurements. However, its use is more feasible in controlled environments, limiting its applicability in specific clinical contexts (Bottaro, 2007; Franciscatto, 2009). An alternative outlined in the Code of Practice TRS/IAEA 457:2007 suggests using non-invasive meters for peak voltage (kVp) measurement (IAEA, 2007). This approach aligns with the latest edition of the standard IEC 61267:2005, which, unlike the previous version, now allows the use of non-invasive meters (INTERNATIONAL ELETROTECHICAL et al., 2005).

Various non-invasive methods have been employed for kVp measurement, providing versatility and practicality, such as those employing X-ray fluorescence and absorption and others based on measuring differential beam attenuation (Fajrin et al., 2019; Vieira et al., 2011). However, these methods are sensitive to variations in beam characteristics and the materials used (typically copper), which can lead to significant deviations in the accurate determination of kVp under real clinical conditions (Vieira et al., 2011; Silva et al., 2000). Additionally, lower precision compared to invasive methods is an important consideration, as external factors such as anode angulation, inherent filtration, and other factors can affect non-invasive measurements, unlike invasive ones (INTERNATIONAL ELETROTECHICAL et al., 2005).

Another non-invasive method determines the maximum X-ray energy, also called the end-point, of a spectrum produced by the tube, which corresponds to the kVp. This method is considered a primary measurement method, as it is based directly on a measurable physical property of the X-ray beam and does not require calibration against an external reference. A linear regression in the final range of the

* Corresponding author.
E-mail addresses: jonathan.rodrigues@aluno.uece.br (J.R. da Silva), murata@alumni.usp.br (H.M. Murata), leonardo.c-riominas@ipen.br (L.C. dos Santos), juan.alcantara.nunez@usp.br (J.A. Alcántara Núñez), vergacas@gmail.com (D.V. de Souza Carvalho), adelsonduarte1@gmail.com (A.D. dos Santos), ubaldobanos@gmail.com (U.B. Rodríguez), mppalbu@ipen.br (M.P.A. Potiens), daniel.bonifacio@ipen.br (D.A.B. Bonifacio).

https://doi.org/10.1016/j.radphyschem.2024.112435
Received 24 July 2024; Received in revised form 23 November 2024; Accepted 26 November 2024
Available online 28 November 2024

bremsstrahlung spectrum, covering a few keV, can be used to determine the kVp (Vieira et al., 2011; Silva et al., 2000; LUCENA and Rodrigo Ferreira de, 2010; Santos, 2017; Terini et al., 2004). Semiconductor detectors play a fundamental role in obtaining X-ray energy spectra.

Those detectors are based on materials such as the commonly used germanium, cadmium telluride, and silicon (Vieira et al., 2011; LUCENA and Rodrigo Ferreira de, 2010; Santos, 2017). In general, they provide excellent energy resolution but are expensive and often require sophisticated electronics and cooling systems to achieve the best performance. In this sense, a cost-benefit approach to addressing these limitations is based on a silicon photomultiplier (SiPM) coupled to a scintillator crystal (Goyal et al., 2017; Grodzicka-et al., 2019; Anjum et al., 2024). The SiPM stands out for its absence of high-power supplies and cooling systems, simplifying handling and integration into more compact and less expensive solutions (Anjum et al., 2024; Acerbi and Gundacker, 2019; Calò et al., 2019).

The SiPM consists of an array of single-photon avalanche diode (SPAD) microcells operating in Geiger mode and connected in parallel. The sensitive area of a SiPM ranges from 1 mm^2 to 6 mm^2 with each microcell varying from 10 μm^2 to 100 μm^2 (Acerbi and Gundacker, 2019; Calò et al., 2019). The size of the microcells should be small enough for only a single photon to be absorbed by each of them. The number of microcells per device ranges from several hundred to several tens of thousands (Acerbi and Gundacker, 2019; Calò et al., 2019).

In a previous work by Terini (Terini et al., 2004), the determination of kVp from the energy spectrum was performed by choosing an ideal energy range to ensure that the linear regression at the end of the spectrum was consistent, by minimizing both the statistical error associated with the kVp value and the parameter χ^2_{red} (reduced chi-square). This work aims to use an improved linear fitting procedure to provide a feasibility study of the use of SiPM coupled to a scintillator in the non-invasive kVp measurement from the energy spectrum, contributing to the advancement of techniques of quality control in radiology.

2. Materials and methods

2.1. Detector

The $Gd_3Al_2Ga_3O_{12}$ scintillator crystal (GAGG, $\rho = 6.6$ g·cm^{-3}, $Z = 54.4$) with dimensions of $4 \times 4 \times 5$ mm^3 was chosen. GAGG possesses a larger attenuation length and shorter decay time when compared to commonly used scintillators in spectroscopy, such as NaI and CsI, and comparable light yield (Gerasymov et al., 2020; Jeong and Hammig, 2020). The GAGG scintillator was enveloped in white Teflon to mitigate the loss of scintillated light photons induced by the incidence of gamma photons and/or X-rays. It was then coupled to the SiPM using Visilox V-788 optical grease, which has a refractive index of 1.463, to enhance the optical coupling between the crystal and the sensor. To maintain the accuracy of the photonic measurements, an opaque shield was fabricated using 3D printing with black polymers. This shield effectively blocks any visible light from penetrating the GAGG-SiPM system, thereby eliminating extraneous light interference that could affect the measurements recorded by the SiPM.

The SiPM used was a Broadcom AFBR-S4N44C013 with an active area of 3.72×3.72 mm^2 and photon detection efficiency (PDE) of 55% at 420 nm, breakdown voltage of 26.9 V. The bias voltage applied to the SiPM was 32 V. To this overvoltage we have a photon detection efficiency (PDE) of 52% at 420 nm, and a gain of 2.5×10^6. The generated electrical signal was amplified, shaped, and processed (BROADCOM, 2023a). The signal readout board was the Broadcom AFBR-S4E001, which provides two signal outputs with 50 Ω impedance, one for photon energy discrimination (Output 1), and another for timing (Output 2) (BROADCOM, 2023b). In this work, only Output 1 was used, featuring an amplification stage in transimpedance configuration.

2.2. Pulse height acquisition and analysis methods

Pulse height discrimination was performed using the open-source Red Pitaya STEMlab 125-10 platform in multichannel analyzer (MCA) mode (Red Pitaya, 2024; Kütt et al., 2018). Hence, Output 1 of the readout board was connected to one of the inputs of the MCA. The pulse was digitized by a 10-bit ADC operating at 125 MSps and passed through a series of digital filters for pulse shaping. Subsequently, the pulse heights were distributed into a histogram to record their frequencies (Red Pitaya, 2024).

The MCA allowed adjustments to several parameters such as Sampling, Bin count, Baseline, Threshold, and Wait time, which were essential to ensure the precise selection and analysis of the pulses of interest (Red Pitaya, 2024). The sampling parameter determined the time between each sample of the signal, allowing for a more detailed representation of rapid pulses. The bin count interval defines the number of intervals used to represent the pulse height distribution, enabling a detailed analysis of the signal amplitude.

The baseline provided a reference point for the average level of the signal before the occurrence of the pulse, which was crucial for distinguishing the signal from background noise. The threshold values defined the amplitude limits of the pulses considered for analysis, avoiding detector saturation, and eliminating unwanted noise. The wait time determined the time the system waited before starting the analysis of the next pulse, ensuring precise analysis without pulse overlap. The numerical values selected for each parameter are shown in Fig. 1.

2.3. Energy calibration

The energy calibration of the detector was performed using emission peaks from the ^{241}Am, ^{133}Ba, and ^{152}Eu sources, as listed in Table 1. These sources provide a direct reference for the energy of the detected radiation, making the calibration method independent of other techniques or external references.

After assembling the equipment, the sources were placed on the detector system for pulse acquisition (Fig. 2).

The radiation spectra emitted by the sources were recorded as a count distribution across channels, with each channel corresponding to an energy range. Gaussian curve fitting was performed to selected energy peaks to determine its channel and resolution. The determination of the channel corresponding to the maximum of the peak will present an error which will be dependent on the data statistics, the energy resolution, and the stability of the detection system. Thus, the calibration curve is obtained from the channel-to-energy dataset by least squares fit, which will introduce errors due to the uncertainties of the coefficients. These errors will be propagated together with the error involved in the process of determining the value of kVp.

2.4. X-ray tube spectroscopy

The experiments with radioactive sources were conducted at the Laboratory of Detectors and Dosimetric Materials (LDMD), while those with X-ray tubes were carried out at the Laboratory of Instruments Calibration (LCI), both at the Nuclear and Energy Research Institute (IPEN/CNEN-SP).

An Agfa ND Pantak/Seifert GmbH & Co. KG., Germany, X-ray radiation system, model Isovolt 160 HS, connected to a Comet X-ray tube, model MRX 160/22, was utilized within the radiology operating range. The radiation field size was limited by lead collimators with 50 mm diameter apertures. The tube voltage was adjusted according to radiodiagnostic and mammography quality standards for attenuated beams used in the LCI, as described in Table 2.

Attenuated beam standards were considered due to the lower value of the Air Kerma Rate compared to direct radiodiagnostic and mammography qualities for direct beams. Elevated Air Kerma Rate is detrimental to pulse detection due to dead time, pulse pile-up, and signal

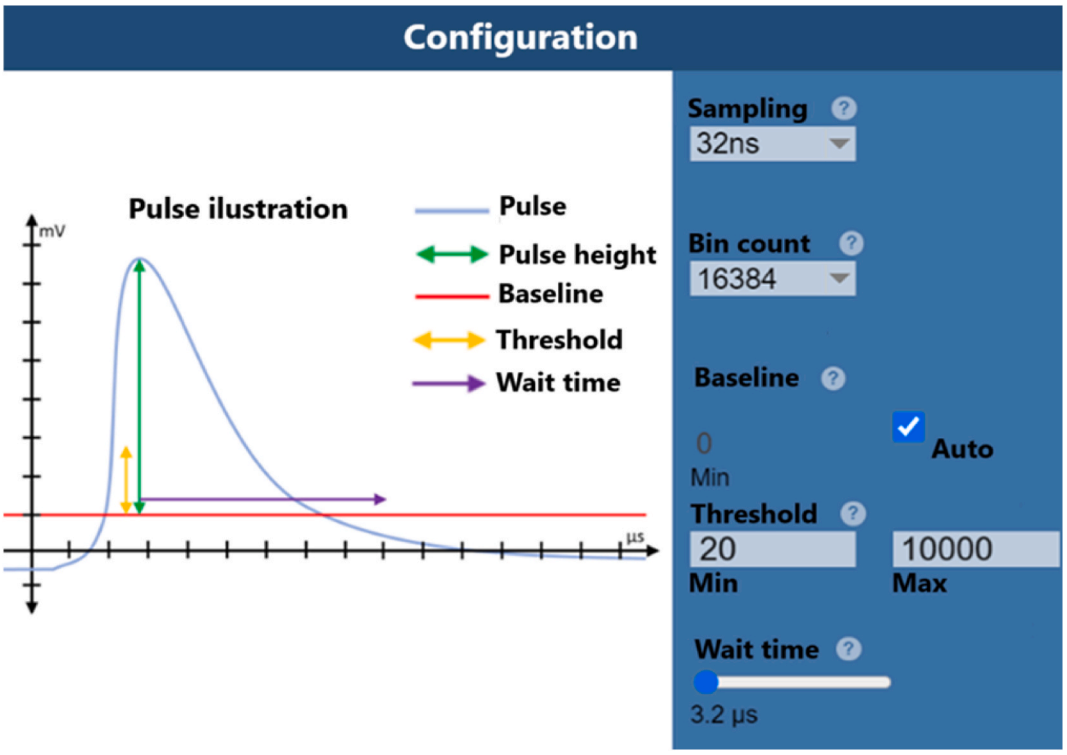

Fig. 1. Adjustable parameters of the pulse height multichannel analyzer (Calò et al., 2019).

Table 1
Characteristics of the isotopes used and main types of emissions (IAEA, 2024).

Isotopes	Activity (kBq)	Date of activity measurement	Energy (keV)	Relative intensity (%)
^{241}Am	311.6	May 09, 2023	17.7	5.7
			59.5	35.9
^{133}Ba	577.3	March 03, 2022	31.0	60.2
			81.0	32.9
^{152}Eu	9.3	April 27, 2023	40.1	37.8
			121.8	28.5

saturation, resulting in poor pulse formation (Vieira et al., 2011; Terini et al., 2004).

To maintain the dead time (3.2 µs) of the detector at a negligible level and not alter the beam quality with the insertion of attenuating filters, it was necessary to keep the detector at a fixed distance of 3 m from the X-ray tube focal point. Additionally, it was necessary to reduce the tube current value from the LCI's practice from 10 mA to 0.1 mA.

For radiation beam monitoring, a PTW ionization chamber, model TW 34014, positioned at the radiation beam outlet after additional filtration, was used. The acquisition time for each spectrum was 30 min to achieve a minimum count of 1000,000 events, considering the Air Kerma Rate for each beam used. The experimental setup configuration is shown in Fig. 3.

A non-invasive kVp meter from Radcal, model Acc-Gold+, which measures the potential applied to the X-ray tube in the range of 50–150 kV with a nominal accuracy of 1.6%, and in the range of 20–40 kV with a nominal accuracy of 2.1%, was used for comparison with our proposed detector.

In the measurements performed with the non-invasive kVp meter, the reference conditions prescribed by the manufacturer were used at a focus-detector distance of 1 m. Due to the impossibility of simultaneous measurements with both the spectrometer system and the non-invasive meter, the substitution method was employed following the recommendations of TRS/IAEA 457:2007 and IEC 61267:2005 for indirect comparison in X-ray tube measurements (IAEA, 2007; INTERNATIONAL ELETROTECHICAL et al., 2005).

2.5. *The method for determining kVp from the energy spectrum*

The maximum X-ray photon energy corresponds to the peak voltage applied to the tube. Thus, identifying the endpoint of the energy spectrum is intrinsically linked to determining the kVp (Terini et al., 2004).

An element that affects the configuration of the final portion of the experimental spectrum is the type of high-voltage generator, directly influencing the ripple value (Terini et al., 2004). Additionally, the final spectrum configuration is also impacted by the pulse pile-up phenomenon, originating from the detector system's dead time, resulting in spectrum extension beyond its maximum energy (Vieira et al., 2011).

The proposed methodology involves fitting a linear function at the final region of the spectrum using raw experimental counts. The kVp value is determined from the intersection of the regression line with the axis of the independent variable (keV).

One of the critical considerations in the method is determining the appropriate energy range limits to be considered in the line fitting. Therefore, we sought to determine the ideal energy interval ($E_{end} - E_{start}$) to ensure that the linear regression at the end of the spectrum was consistent, aiming to minimize both the statistical error (σ_d) associated with the kVp value and the χ^2_{red} used to quantify the fit quality.

The potential calculation starts by selecting an energy value lower than E_{end}, near the end of the spectrum. Next, an energy value E_{kVp} is estimated for the abscissa of the spectrum's endpoint. Linear regression is performed in this region using the least squares method. Iterations are carried out, varying E_{kVp}, until the regression-determined value E_{kVp} is approximately equal to E_{start}.

The regression is calculated using a 10 keV range for all spectra. For each E_{kVp} value, the respective σ_d and χ^2_{red} are determined, similar to the study conducted in (Terini et al., 2004), where the kVp value is obtained from the X-ray spectrum using a PIN photodiode as a detector. The value of P_α was evaluated to verify the optimal fit condition for the linear

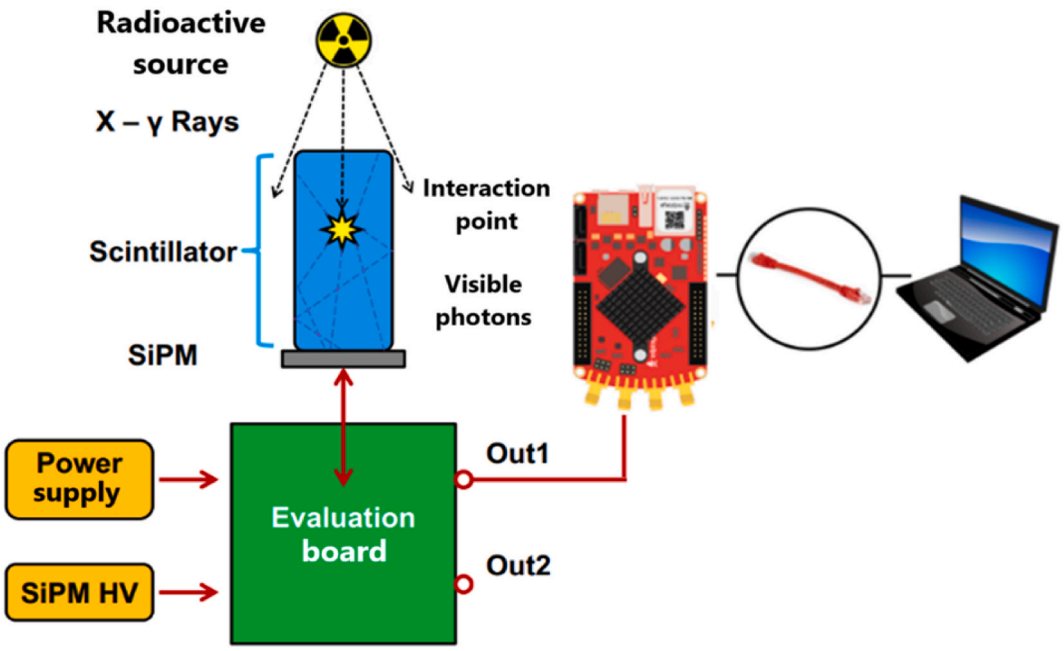

Fig. 2. Configuration of the experiment with radioactive sources.

Table 2
Radiodiagnostic and mammography quality for attenuated beams.

Beam quality	kV	HVL (mm of Al)	Additional filtration (mm of Al)
RQA-3	50	3.8	12.4
RQA-5	70	6.8	23.8
RQA-8	100	10.1	37.3
RQA-10	150	13.3	49.2
RQA-M2	28	0.6	2.0 + 0.07 (Mo)
RQA-M4	35	0.9	2.0 + 0.07 (Mo)

regression. The value of P_α is the product of σ_d and the respective χ^2_{red} for the E_{kVp} values.

3. Results and discussions

3.1. Spectroscopy with radioactive sources

Fig. 4 shows the spectra of ^{241}Am, ^{133}Ba, and ^{152}Eu used in the detector calibration. Lowest energy peaks present the poorest resolution. The energy resolutions of the selected peaks of these spectra were calculated, as shown in Table 3 and the graphical representation of the energy resolution versus energy in Fig. 5.

The electronic circuitry employed plays a significant role in the spectrometer's resolution (Santos, 2017). The energy resolution values obtained at 60 keV and 122 keV align with a previous work also utilizing SiPM coupled with GAGG:Ce (Kataoka et al., 2015; Sibczynski et al., 2015).

A calibration curve has been formulated and is depicted in Fig. 6. Regarding the detector system calibration, the straight line exhibited a significant outcome, with satisfactory coefficients of the line. A slight variation in the slope coefficient of the line was observed across the set of measurements, demonstrating the consistency of the method used.

The good linearity of the calibration curve aligns with findings from other studies that used GAGG coupled with SiPM (Jeong and Hammig, 2020). Despite the nonlinear effects associated with GAGG's light yield, which impact the scintillator's spectroscopic response (Sibczynski et al., 2015; Campana et al., 2023), these were not sufficient to affect the linear

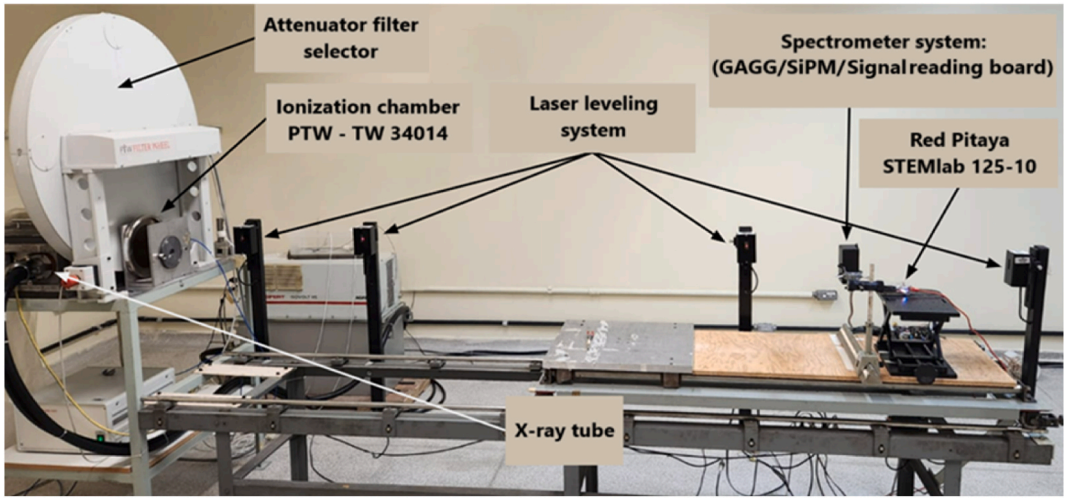

Fig. 3. – Experimental setup with the X-rays beam.

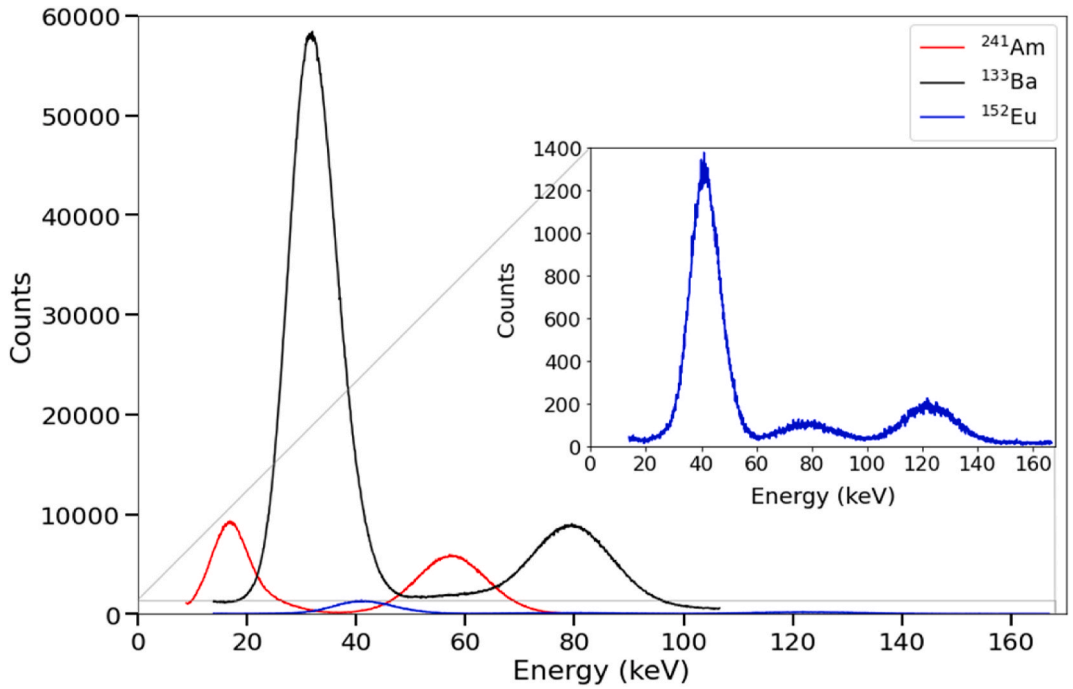

Fig. 4. – Energy spectra of ^{241}Am, ^{133}Ba, and ^{152}Eu.

Table 3
– Correlation of channel, FWHM, and energy resolution (%) for each peak of the calibration sources.

Isotopes	Energy (keV)	Channel (centroid)	FWHM (keV)	Resolution (%)
^{241}Am	17.7	134.6 ± 0.2	10.9 ± 0.1	61.4 ± 0.3
	59.5	571.2 ± 0.1	16.9 ± 0.0	28.5 ± 0.3
^{133}Ba	31.0	297.4 ± 0.2	11.7 ± 0.0	37.8 ± 0.1
	81.0	809.1 ± 0.1	18.2 ± 0.0	22.5 ± 0.1
^{152}Eu	40.1	397.9 ± 0.2	13.9 ± 0.0	34.8 ± 0.0
	121.8	1275.3 ± 0.6	22.4 ± 0.2	18.4 ± 0.0

behavior of the calibration curve. Similarly, the nonlinear effects associated with SiPM, such as photon rate, pixel recovery time, and correlated and uncorrelated noise (dark count, crosstalk, and after pulses) (Acerbi and Gundacker, 2019; Moya-et al., 2024), did not significantly influence the results.

3.2. X-ray tube spectroscopy

For the determination of kVp from the energy spectrum, one of the critical considerations in the linear regression method is determining the appropriate energy range limits to be considered in the line fitting. If the energy range is wide, it is possible to obtain a divergent kVp value, even with low statistical uncertainty, because the line defined by the linear regression model would not be a good description. On the other hand, if the energy interval is too narrow, the line fitting may have better convergence to the true value, but the kVp value will have a high standard deviation, resulting from the decreased number of considered points.

Table 4 presents the comparison of the results obtained for determining the energy range to obtain the kVp, aiming to minimize both the statistical error associated with the kVp value and the parameter χ^2_{red}, used to quantify the fit quality. Additionally, the table includes the energy range that presents the lowest P_α value, used to verify the optimal fit condition for the linear regression.

It was evidenced that using an energy range of 3.0 keV, with each energy interval having a width of 0.1 keV, for the linear adjustment in the final region of the spectrum is sufficient to accurately determine the kVp value. Reduced chi-squared values of up to 1.44 were obtained, indicating that the model fits the data well. Additionally, this energy range presents the lowest P_α value for most beam qualities.

The product P_α is justified by the fact that, as we increase the number of points for the adjustment, the standard deviation values σ_d decrease, unlike the values of χ^2_{red}, which increases because the adjustment starts to encompass points that do not form a straight line. However, with the use of theses analytical methods, a variation in the energy range would be necessary to obtain the smallest product value, as shown in Table 4.

X-ray spectra were obtained using the calibrated detector. For the acquired X-ray spectra, the maximum number of counts in a single channel was 100,000, indicating good statistics for kVp determination. Fig. 7 shows the spectra RQA 3, 5, 8, 10, M2, and M4, as well as their respective linear regression lines applied to the final regions of the spectra.

Table 5 shows the obtained parameters with the X-ray equipment. An energy range of 3.0 keV was used for applying the linear regression in the final spectrum region. The width of each energy interval was established at 0.1 keV, which was adopted for the linear fit.

Table 6 details the results obtained by the developed spectrometer, the non-invasive monitoring system Accu Gold, and from other studies conducted at the LCI previously. The reference studies used commercial spectrometers using HPGe (LUCENA and Rodrigo Ferreira de, 2010) and CdTe (Santos, 2017) detectors and the non-invasive meter Diavolt (LUCENA and Rodrigo Ferreira de, 2010) with different experimental configurations and beam qualities.

Based on these results, we obtained the percentage differences between the SiPM/GAGG spectrometer and other systems and non-invasive meters, for each beam quality, as presented in Fig. 8.

In relation to the non-invasive measurements performed by the Accu Gold, percentage errors above the limit (<5%), recommended by the standard IEC 61676:2005 and TRS/IAEA 457:2007 for beams below ≤50 kV, were found. For commercial spectrometers, percentage deviations above 5% were obtained for the 35 and 50 kVp beams. The non-invasive meter Diavolt presented deviations below 5%.

In the comparative results presented in Table 6 and Fig. 8, it is shown that despite the use of different spectrometer systems (HPGe and CdTe)

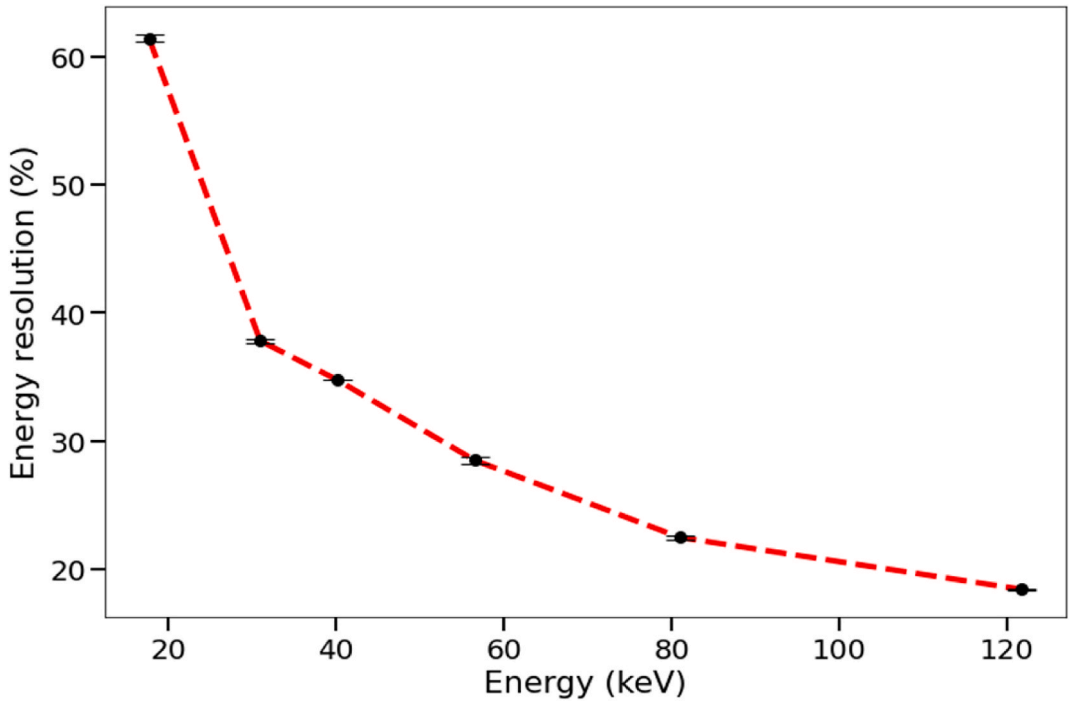

Fig. 5. Energy resolution (%) vs. Energy (keV).

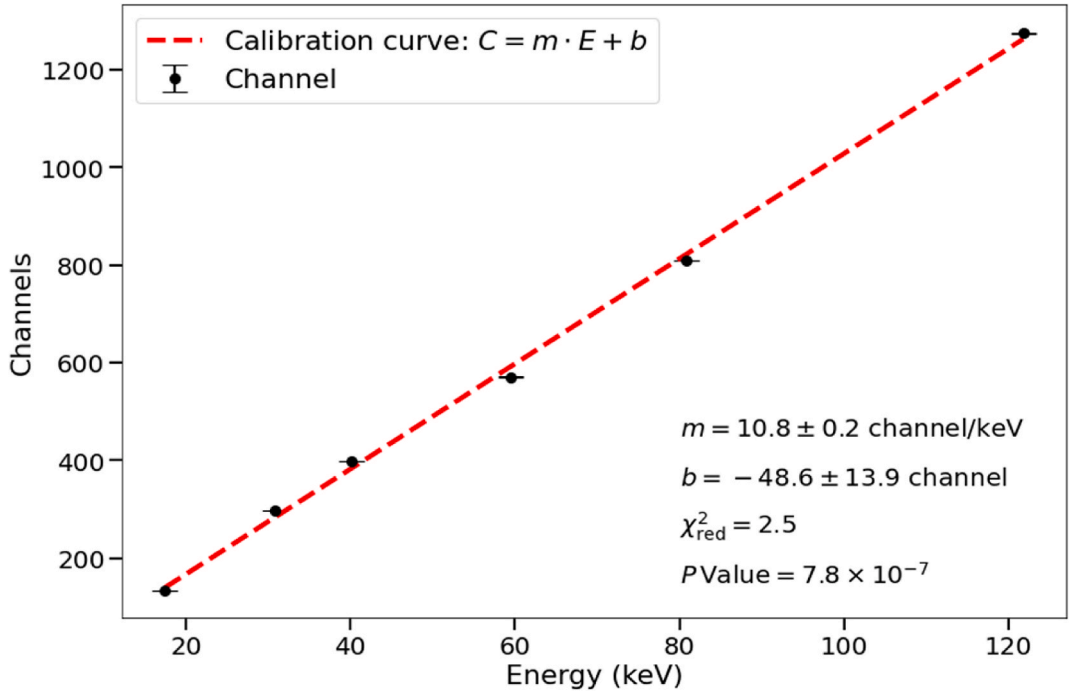

Fig. 6. Calibration curve obtained from spectral results.

in previous works (Silva et al., 2000; LUCENA and Rodrigo Ferreira de, 2010), which are widely used in X-ray and gamma spectroscopy, the results were considerably similar compared to the results obtained with the spectrometer system used in this work.

However, the use of SiPM coupled with the GAGG crystal compared to CdTe and HPGe detectors stands out due to the absence of the need for high voltage sources and cooling systems, simplifying handling and integration into more compact systems. Additionally, its radiation resistance and lower sensitivity to temperature represent an additional advantage.

4. Conclusion

This study evaluated the feasibility of using a silicon photomultiplier (SiPM) coupled to a scintillator for the non-invasive measurement of kVp in a typical X-ray beam. The X-ray spectra acquired with the spectrometer system: GAGG, SiPM (AFBR-S4N44P014 M), AFBR-S4E001 kit, and MCA, allow for the practical determination of the real energy

Table 4
Energy values (kVp), χ^2_{red}, and P_α for different energy ranges.

Beam quality	Energy range: 3.5 keV			Energy range: 3.0 keV			The minimum value of P_α			
	kVp	χ^2_{red}	P_α	kVp	χ^2_{red}	P_α	kVp	χ^2_{red}	P_α	keV
RQA-3	54.3 ± 0.6	2.7	1.5	54.4 ± 0.5	1.4	0.8	54.4 ± 0.5	1.4	0.8	3.0
RQA-5	70.5 ± 0.7	1.1	0.7	70.6 ± 0.8	1.0	0.9	70.5 ± 0.7	1.1	0.7	3.5
RQA-8	100.7 ± 1.7	1.3	2.1	100.8 ± 1.9	1.0	1.9	100.2 ± 0.5	1.6	0.8	8.5
RQA-10	150.7 ± 5.1	1.3	6.5	150.8 ± 6.5	1.3	8.3	149.4 ± 1.1	1.4	1.6	10.0
RQA-M2	29.8 ± 0.2	1.3	0.3	29.8 ± 0.2	1.0	0.2	29.8 ± 0.2	1.0	0.2	3.0
RQA-M4	39.9 ± 0.2	1.3	0.3	39.8 ± 0.3	1.1	0.3	39.8 ± 0.3	1.1	0.3	3.0

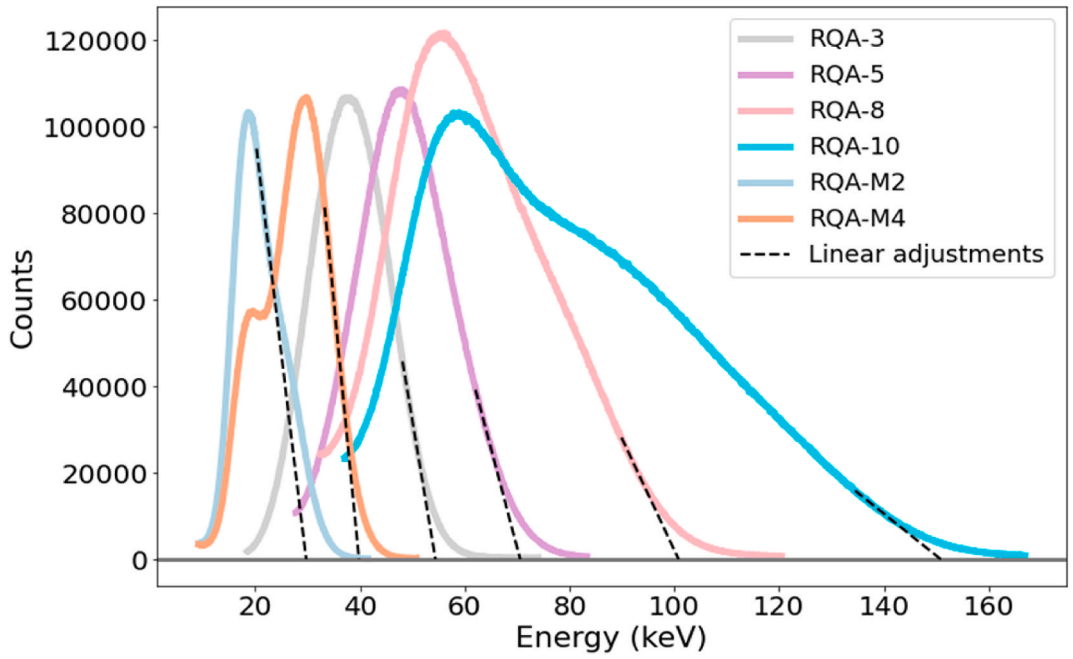

Fig. 7. Spectra and their respective linear regression lines.

Table 5
Obtaining the kVp for the attenuated beam qualities used.

Beam quality	kV	Channel (centroid)	Stipulated kVp (E = (C-b)/m)	χ^2_{red}
RQA-3	50	537.7 ± 1.4	54.4 ± 0.5	1.4
RQA-5	70	711.8 ± 8.5	70.6 ± 0.8	1.0
RQA-8	100	1037.5 ± 19.7	100.8 ± 1.9	1.0
RQA-10	150	1576.2 ± 67.7	150.8 ± 6.5	1.3
RQA-M2	28	271.9 ± 2.1	29.8 ± 0.2	1.0
RQA-M4	35	380. 5 ± 2.5	39.8 ± 0.3	1.1

spectrum of X-rays.

However, for different types of measurement systems, particularly for low-energy beams (35–50 kVp the results clearly exceed the percentage error limit (<5%) recommended by IEC 61676:2005 and TRS/IAEA 457:2007. The highest percentage differences were obtained below 40 keV, which could reflect the poor energy resolution for this energy range since it affects the shape at the end of the spectrum.

The comparative analysis showed that while commercial CdTe and HPGe detectors are effective, the SiPM coupled with the GAGG crystal is a viable alternative. However, it is necessary to address the observed deficiencies before its clinical use. Improvements in energy resolution will be necessary, especially for applications like mammography, to meet the required quality standards.

One way to address the poor energy resolution at energies below 40 keV and achieve better results in kVp measurement is to implement bias voltage control as a function of temperature to stabilize the SiPM gain (Ivanovs et al., 2019; Kuznetsov, 2018). The use of new and improved SiPM models, which have a photon detection efficiency (PDE) of 63% at 420 nm, along with reduced crosstalk and dark count rates, can further enhance performance (BROADCOM, 2024).

The use of attenuating filters, which reduce the photon rate at the

Table 6
Comparison of the results of the proposed spectrometer with previous studies conducted at the Instrument Calibration Laboratory - LCI/IPEN-SP using commercial HPGe (LUCENA and Rodrigo Ferreira de, 2010) and CdTe (Santos, 2017) spectrometers.

Nominal voltage (kV)	Measurement (Accu Gold+)	Measurement (Diavolt)	kVp (SiPM/GAGG)	kVp (HPGe)	kVp (CdTe)
50	51.5 ± 0.8	52.5 ± 1.4	54.4 ± 0.5	51.3 ± 0.9	51.8 ± 3.6
70	71.2 ± 1.1	72.4 ± 1.9	70.6 ± 0.8	71.3 ± 1.1	71.6 ± 2.2
100	103.7 ± 1.7	102.9 ± 2.6	100.8 ± 1.9	101.5 ± 1.1	101.8 ± 1.8
150	153.6 ± 2.5	–	150.8 ± 6.5	151.3 ± 1.1	150.0 ± 0.0
28	27.7 ± 0.6	–	29.8 ± 0.2	29.2 ± 1.0	29.5 ± 5.5
35	34.5 ± 0.7	–	39.8 ± 0.3	36.2 ± 0.7	36.8 ± 5.2

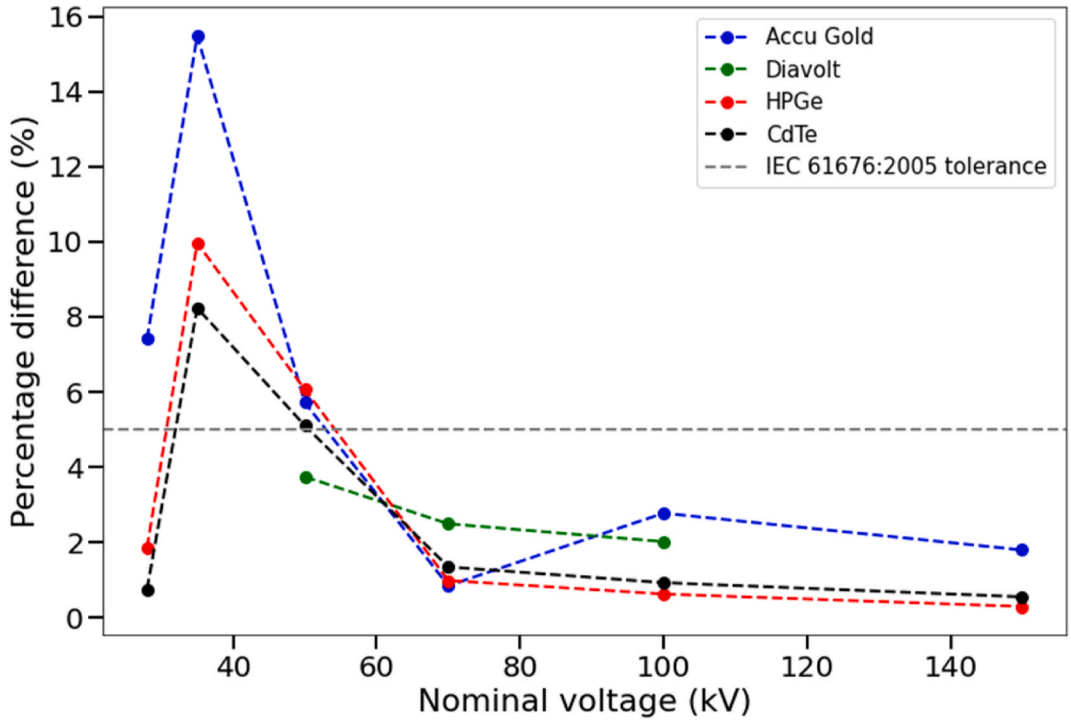

Fig. 8. Percentage differences between the SiPM/GAGG spectrometer system and other measurement systems.

detector and allow for a shorter distance between the X-ray tube and the detector, optimizes kVp measurement under clinical conditions without compromising accuracy. Furthermore, the use of artificial intelligence improves the identification of the spectrum's endpoint, distinguishing noise from true signals and adapting to variations caused by fluctuations in the tube or experimental conditions (Deumel et al., 2021; Pang et al., 2022).

CRediT authorship contribution statement

Jonathan Rodrigues da Silva: Writing – review & editing, Writing – original draft, Visualization, Validation, Methodology, Investigation, Data curation. **Helio Massaharu Murata:** Writing – review & editing, Validation, Supervision, Methodology, Funding acquisition, Data curation. **Leonardo Camargo dos Santos:** Writing – review & editing, Methodology, Data curation. **Juan Antonio Alcántara Núñez:** Writing – review & editing, Methodology, Data curation. **Diego Vergaças de Souza Carvalho:** Writing – review & editing, Methodology, Data curation. **Adelson Duarte dos Santos:** Writing – review & editing, Methodology, Data curation. **Ubaldo Baños Rodríguez:** Writing – review & editing, Methodology, Data curation. **Maria da Penha Albuquerque Potiens:** Writing – review & editing, Resources, Methodology. **Daniel Alexandre Baptista Bonifacio:** Writing – review & editing, Validation, Supervision, Resources, Project administration, Methodology, Funding acquisition, Data curation, Conceptualization.

Declaration of competing interest

The authors declare that they have no known competing financial interests or personal relationships that could have appeared to influence the work reported in this paper.

Acknowledgments

All authors declare that they have no known conflicts of interest in terms of competing financial interests or personal relationships that could have an influence or are relevant to the work reported in this paper.

This work has been in part supported by the Brazilian funding agencies Conselho Nacional de Desenvolvimento Científico e Tecnológico (CNPq grant agreement Nº 202378/2020–9 and 435039/2018–0) and Financiadora de Estudos e Projetos (FINEP grant agreement Nº 0294/16). We also acknowledge the support from the São Paulo Research Foundation (FAPESP) under grant #2023/00079–8.

Data availability

Data will be made available on request.

References

Acerbi, F., Gundacker, S., 2019. Understanding and simulating SiPMs. Nucl. Instrum. Methods Phys. Res., Sect. A: Accelerators, Spectrometers, Detectors and Associated Equipment, Silicon Photomultipliers: Technology, Characterisation and Applications 926, 16–35.

AGENCY, I. A. E, 2023. Handbook of Basic Quality Control Tests for Diagnostic Radiology. International Atomic Energy Agency. https://www-pub.iaea.org/MTCD/Publications/PDF/PUB2021_web.pdf. . (Accessed 12 November 2023).

Anjum, F., et al., 2024. Characterization and performance of SiPM-CsI(Tl) detector for low-energy γ - and X-ray spectroscopy. Radiat. Phys. Chem. 216, 111442.

Bottaro, M., 2007. Estudo do envelhecimento de um tubo de Raios-X por métodos não invasivos. Universidade de São Paulo.

BRASIL. Agência Nacional de Vigilância Sanitária. Resolução RDC no 611, de 9 de março de, 2022. Aprova o Regulamento Técnico sobre os requisitos de qualidade de equipamentos e materiais utilizados em radiologia médica. Diário Oficial da União: seção 1, Brasília, DF, p. 107, 9 mar. 2022. https://www.in.gov.br/en/web/dou/-/resolucao-rdc-n-611-de-9-de-marco-de-2022-386107075. . (Accessed 12 November 2023).

BROADCOM, 2023a. AFBR-S4N44P014M: NUV-HD Single Silicon Photo Multiplier.

BROADCOM, 2023b. AFBR-S4E001: Evaluation Kit for the AFBR-S4NxxPyy4M SiPM Family.

BROADCOM, 2024. AFBR-S4N44P014M: NUV-MT Silicon Photomultiplier.

Calò, P.P., et al., 2019. SiPM readout electronics. Nucl. Instrum. Methods Phys. Res., Sect. A: Accelerators, Spectrometers, Detectors and Associated Equipment, Silicon Photomultipliers: Technology, Characterisation and Applications 926, 57–68.

Campana, R., et al., 2023. Measurement of the non-linearity in the γ-ray response of the GAGG:Ce inorganic scintillator. Nucl. Instrum. Methods Phys. Res. Sect. A Accel. Spectrom. Detect. Assoc. Equip. 1056, 168587.

Deumel, S., et al., 2021. High-sensitivity high-resolution X-ray imaging with soft-sintered metal halide perovskites. Nature Electronics 4 (9), 681–688.

Fajrin, H.R., Rahmat, Z., Sukwono, D., 2019. Kilovolt peak meter design as a calibrator of X-ray machine. Int. J. Electr. Comput. Eng. 9, 2328.
Franciscatto, P.C., 2009. Caracterização das qualidades de radiação X seguindo as recomendações da norma IEC 61267 no laboratório de calibração do IPEN. Mestrado em Tecnologia Nuclear - Aplicações. Universidade de São Paulo, São Paulo, 16 set.
Gerasymov, I., et al., 2020. GAGG: Ce composite scintillator for X-ray imaging. Opt. Mater. 109, 110305.
Goyal, S.K., et al., 2017. Design & Development of Position Sensitive Detector for Hard X-Ray Using SiPM and New Generation Scintillators.
Grodzicka-Kobylka, M., Moszyński, M., Szczęśniak, T., 2019. Silicon photomultipliers in gamma spectroscopy with scintillators. Nucl. Instrum. Methods Phys. Res., Sect. A: Accelerators, Spectrometers, Detectors and Associated Equipment, Silicon Photomultipliers: Technology, Characterisation and Applications 926, 129–147.
IAEA, 2007. In: Dosimetry in Diagnostic Radiology: an International Code of Practice. International Atomic Energy Agency, Vienna.
IAEA, 2021. Protocolos de Control de Calidad para Radiodiagnóstico en América Latina y el CaribeProtocolos de Control de Calidad para Radiodiagnóstico en América Latina y el Caribe. International Atomic Energy Agency. https://www.iaea.org/es/publications/14712/protocolos-de-control-de-calidad-pararadiodiagnostico-en-america-latina-y-el-caribe. (Accessed 12 November 2023).
IAEA, 2024. LiveChart of nuclides, © 2009 - 2024. IAEA Nuclear Data Section. https://www-nds.iaea.org/relnsd/vcharthtml/VChartHTML.html. . (Accessed 18 July 2024).
INTERNATIONAL ELETROTECHICAL COMMISSION. IEC 61267:2005, 2005. Medical Diagnostic X-Ray Equipment – Radiation Conditions for Use in the Determination of Characteristics. Geneva.
Ivanovs, V., et al., 2019. TEMPERATURE STABILIZATION OF SiPM-BASED GAMMA-RADIATION SCINTILLATION DETECTORS. RAD Association Journal 3 (3).
Jeong, M., Hammig, M., 2020. Development of hand-held coded-aperture gamma ray imaging system based on GAGG(Ce) scintillator coupled with SiPM array. Nucl. Eng. Technol. 52 (11), 2572–2580.
Kataoka, J., et al., 2015. Recent progress of MPPC-based scintillation detectors in high precision X-ray and gamma-ray imaging. Nucl. Instrum. Methods Phys. Res., Sect. A: Accelerators, Spectrometers, Detectors and Associated Equipment, Symposium on Radiation Measurements and Applications 2014 (SORMA XV) 784, 248–254.
Kütt, M., Göttsche, M., Glaser, A., 2018. Information barrier experimental: toward a trusted and open-source computing platform for nuclear warhead verification. Measurement 114, 185–190.
Kuznetsov, E., 2018. Temperature-compensated silicon photomultiplier. Nucl. Instrum. Methods Phys. Res. Sect. A Accel. Spectrom. Detect. Assoc. Equip. 912, 226–230. New Developments In Photodetection 2017.
LUCENA, Rodrigo Ferreira de, 2010. Implantação de um programa de controle de qualidade em equipamentos de raios x por meio de medidores não invasivos. Dissertação (Mestrado) – Universidade de São Paulo, São Paulo, 2010.
Moya-Zamanillo, V., Rosado, J., 2024. Understanding the nonlinear response of SiPMs. Sensors 24 (8), 2648. Basel, Switzerland.
Pang, J., et al., 2022. Vertical matrix perovskite X-ray detector for effective multi-energy discrimination. Light Sci. Appl. 11 (1), 105.
Red Pitaya, 2024. Red Pitaya Documentation: Release 0.97, 2024. https://redpitaya.readthedocs.io/en/latest/ (Accessed 20 November 2023).
Santos, L.R.D.O.S., 2017. Desenvolvimento de um protocolo de calibração utilizando espectrometria e simulação matemática, em feixes padrões de raios x. Universidade de São Paulo.
Sibczynski, P., et al., 2015. Characterization of GAGG:Ce scintillators with various Al-to-Ga ratio. Nucl. Instrum. Methods Phys. Res. Sect. A Accel. Spectrom. Detect. Assoc. Equip. 772, 112–117.
Silva, M.C., et al., 2000. Determination of the voltage applied to x-ray tubes from the bremsstrahlung spectrum obtained with a silicon PIN photodiode. Med. Phys. 27 (11), 2617–2623.
Terini, R.A., et al., 2004. Comprehensive analysis of the spectrometric determination of voltage applied to X-ray tubes in the radiography and mammography energy ranges using a silicon PIN photodiode. Br. J. Radiol. 77 (917), 395–404.
Vieira, A.A., et al., 2011. A portable Compton spectrometer for clinical X-ray beams in the energy range 20 150keV. Appl. Radiat. Isot. 69, 350–357. https://doi.org/10.1016/j.apradiso.2010.10.011 [online].